Proceedings of the ASME 2010 3rd Joint US-European Fluids Engineering Summer Meeting and 8th International Conference on Nanochannels, Microchannels, and Minichannels
FEDSM-ICNMM2010
August 1-5, 2010, Montreal, Canada

FEDSM-ICNMM2010-30698

ISOTHERMAL MODELING OF MENISCUS OSCILLATION IN THE CONTINUOUS STRIP CASTING PROCESS

Kevin W. Wilcox
Department of Mechanical Engineering
University of New Brunswick
Fredericton, New Brunswick E3B 5A3
Email: k.wwilcox@unb.ca

A. Gordon L. Holloway
Department of Mechanical Engineering
University of New Brunswick
Fredericton, New Brunswick E3B 5A3
Email: holloway@unb.ca

Andrew. G. Gerber
Department of Mechanical Engineering
University of New Brunswick
Fredericton, New Brunswick E3B 5A3
Email: agerber@unb.ca

ABSTRACT

In the continuous strip casting process a meniscus forms a compliant boundary between the casting nozzle and transporting conveyor. Movement of this meniscus during casting has been shown to create surface defects, which require extensive cold work to remove and limit the minimum thickness for which sections may be cast. This paper discusses experimental work conducted to test an analytical model of the meniscus oscillation. A high frame rate shadowgraph technique was used on an isothermal water model of the casting process to observe meniscus motion, and thus allowing the calculation of meniscus frequency, amplitude, contact points and contact angles. Both natural frequency and flow excited tests were conducted. Natural frequency tests were also conducted using mercury as the working fluid, having a non-wetting contact angle, typical of molten metals. The experimental results were found to be in good agreement with the predictions of theory for both wetting and non-wetting conditions. The experimentally verified analytical model for meniscus motion is valuable to the design of the continuous casting process, because it offers an opportunity to mitigate the effects of boundary motion on surface quality.

NOMENCLATURE

A_{cv}	Control area in analytical theory	m^2
D_{h_2}	Hydraulic diameter post step	m
d	Channel depth (width)	m
E	Meniscus fluctuation energy	J
f_n	Meniscus natural frequency	Hz
F_u	Probability density function of u	$-$
g	Acceleration due to gravity	m/s^2
H	Static head at the meniscus	m_{H2O}
h	Step height	m
$h_{1,2}$	Pre/post-step channel height	m
h_{eff}	Effective step height for recessed meniscus	m
I	Dimensionless inertia term (slenderness)	$-$
L	Channel length	m
Δp	Pressure difference across the meniscus	Pa
q	Channel flow rate per unit depth	m^2/s
R	Meniscus radius	m
t	Time	s
U	Average velocity in channel	m/s
u	Fluctuations in average velocity U	m/s
$x_{c,s}, y_{c,s}$	Meniscus contact points, relative to step edge	m
z	Velocity fluctuations normalized by σ_u	$-$
β	Taper angle of step edge	deg
η	Dimensionless meniscus head	$-$
θ	Caster angle	deg
κ	Meniscus curvature (inverse radius)	$1/m$
λ	Contact angle hysteresis	$-$
ν	Kinematic viscosity	m^2/s
ρ	Density	kg/m^3
σ	Surface tension	N/m
σ_u	Standard deviation of velocity fluctuations, u	m/s
ϕ	Equilibrium contact angle	deg
$\phi_{a,e,r}$	Advancing/average/receding contact angle	deg
ψ	Dimensionless meniscus stiffness	$-$
Ω_n	Dimensionless meniscus frequency	$-$

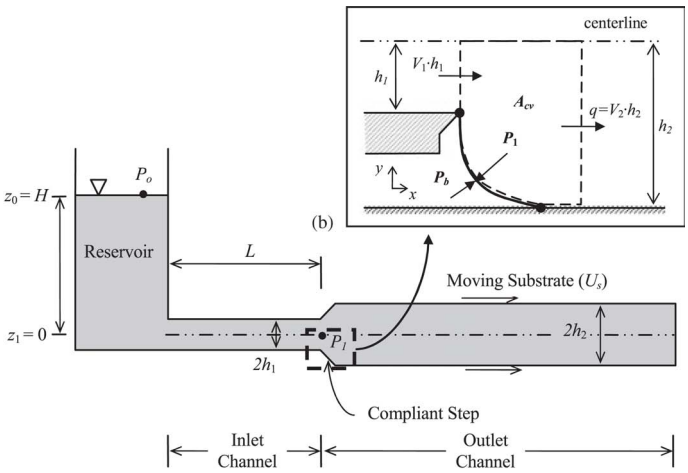

FIGURE 1. GEOMETRY OF THE STRIP CASTING PROCESS SHOWING THE ALUMINIUM-AIR MENISCUS WHICH FORMS BETWEEN THE CASTING NOZZLE EXIT AND TRANSPORTING CONVEYOR.

PROBLEM INTRODUCTION

The problem to be investigated is that of the flow over a backward facing step where the step face is spanned by a liquid-air meniscus that is free to respond to pressure changes in the flow. The motivation for this project originates in the aluminium continuous strip casting process where molten aluminium forms a meniscus with air between the casting nozzle and the moving conveyor which transports the solid product downstream, see Fig. 1. Oscillations of this meniscus are believed to be responsible for imperfections in the final aluminium cast.

An isothermal, geometrically similar, air-liquid meniscus on a stationary substrate was used to model this flow and provide insight into the meniscus oscillation phenomenon. The effect of different geometric properties on the frequency of meniscus motion will be determined and compared to an analytical theory [1, 2]. In particular, this paper will discuss the effects of channel slenderness and contact angle on the natural frequency of the meniscus. The effect of liquid velocity on the frequency and amplitude of meniscus motion in the presence of continuous flow will also be studied.

ANALYTICAL MODEL

Natural Frequency

A model for meniscus natural frequency in the horizontal strip casting process was developed [1, 2], based on the unsteady Bernoulli equation and the Young-Laplace equation for the meniscus surface, using the geometry shown in Fig. 1.

$$f_n = \frac{1}{2\pi}\sqrt{\frac{h_1}{\rho L}\left(\sigma \frac{d\kappa}{dA_{cv}}\bigg|_{eq} + \frac{\rho g}{h}\sin\theta\right)} \tag{1}$$

Equation 1 applies to an angled casting configuration where the outlet flow rate of solidified metal is fixed as in the industrial process.

For the isothermal water model the inflow rate will be fixed rather than the outflow for practical reasons. The only adjustment required in Eqn. 1 to accommodate this change is the replacement of h_1 with h_2 and the association of length L with the outlet channel length, as opposed to the inlet channel length, as defined in Fig. 1. The angle θ is the casting angle measured with respect to the horizontal. In the casting case, oscillations due to meniscus motion occur in the inlet channel; whereas in the present model fluid oscillations occur in the outlet channel.

Equation 1, with the discussed changes to channel height and length, may also be expressed in dimensionless terms for the purpose of empirical fitting to the data.

$$\Omega_n = \sqrt{I(\psi + Bo)} \tag{2}$$

where

$$I = \frac{h_2}{L} \qquad \psi(\eta,\phi) = h_{eff}^3 \frac{d\kappa}{dA_{cv}} \qquad Bo = \frac{Fr}{We} = \frac{\rho g h_{eff}^2}{\sigma}$$

$$\eta = \kappa h_{eff} \qquad \Omega_n = 2\pi f_n \sqrt{\frac{\rho h_{eff}^3}{\sigma}}$$

In this form there are three important parameters for determining the meniscus frequency, the channel slenderness, I, meniscus stiffness, ψ and the Bond number, Bo. Of these three, the slenderness and Bond number can be easily determined from the geometry of the caster. The stiffness, however, depends on the dimensionless head, η, and the contact angle, ϕ.

Meniscus Stiffness

The meniscus of Fig. 2 is defined by its curvature, κ, the horizontal contact points, x_c and x_s, the step height, h, and the step inclusion angle, β. The upper contact point may be at the edge (0,0) or, as indicated in the figure, recessed under the step where the nominal step height, h, is replaced with the effective step height, h_{eff}.

The meniscus stiffness contains the curvature-area derivative, $d\kappa/dA_{cv}$, which can be calculated numerically by computing the change in area behind the meniscus, A_{cv}, for two

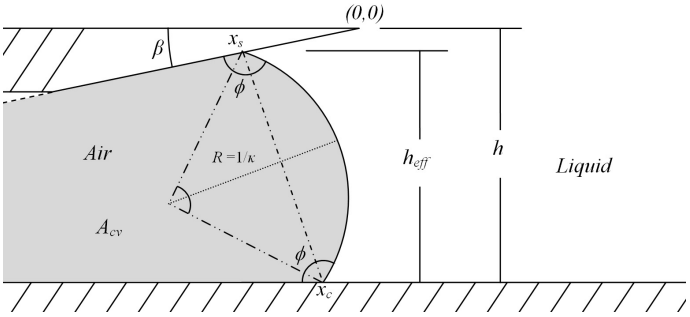

FIGURE 2. POSITION OF THE MENISCUS BETWEEN THE CASTING NOZZLE EXIT AND THE MOVING CONVEYOR. THE UPPER MENISCUS EDGE MAY ATTACH TO THE STEP EDGE OR RECESS AS SHOWN.

slightly different curvatures, κ^+ and κ^-, which are infinitesimally greater and smaller than the equilibrium curvature, κ. The functional form of this derivative is shown in Eqn. 3.

$$\frac{d\kappa}{dA_{cv}} = \frac{\kappa(\phi^+, x_c^+, x_s^+, h, \beta) - \kappa(\phi^-, x_c^-, x_s^-, h, \beta)}{A_{cv}(\phi^+, x_c^+, x_s^+, h, \beta) - A_{cv}(\phi^-, x_c^-, x_s^-, h, \beta)} \quad (3)$$

As Eqn. 3 indicates, the curvature, and hence the value of the derivative, depends on the movement of the contact lines, contact angles or both. We will close this model using two limiting cases for meniscus motion; one in which the contact line remains stationary and the contact angle changes and the other where the contact angle remains constant and the contact line moves. Both result in changes to meniscus curvature. These two scenarios are illustrated for clarity in Fig. 3 and Fig. 4 respectively.

The meniscus stiffness, for both contact point models, is calculated as a function of the dimensionless head, η, and the meniscus contact angle, ϕ; the inclusion angle, β, is 20^o for all experiments and theoretical calculations. Figures 6 and 7 show the stiffness results for the fixed contact line and the fixed contact angle models respectively. It is interesting to note for both models that when the upper meniscus contact point rests on the step edge, a range of stiffnesses is possible for the one contact angle; however, when the meniscus is recessed, the stiffness becomes a singular value with contact angle; this is due to the geometric similarity of all the recessed cases. The stiffness curves are symmetric about $\eta = 0$ for the wetting and non-wetting cases up to the point where the non-wetting curves end abruptly because the upper contact angle, when the meniscus is on the step edge, is free to assume any angle in the wetting case (the case depicted in Fig. 2), but it is restricted in the non-wetting case since the meniscus contact angle ϕ must be less than $90^o - \beta$. Comparing Fig. 6 and Fig. 7 we find that the stiffness is approximately three to four times greater for the fixed contact line model. The cases investigated in this paper are all recessed; the stiffness as a function of equilibrium contact angle for the recessed condition is shown in Fig. 5. The points in Fig. 5 correspond to the recessed points of Figs. 6 and 7. True meniscus motion may be a mixture of contact line and contact angle motion where the stiffness would fall between the limits shown in Fig. 5, imposed by the two motion models.

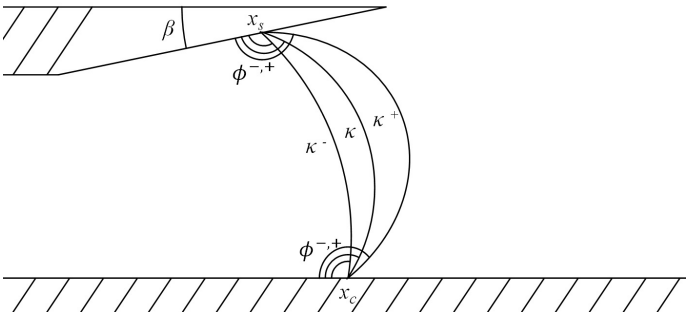

FIGURE 3. MENISCUS MOTION WHEN THE CONTACT LINE IS FIXED AND CURVATURE CHANGE IS ACCOMMODATED BY A CHANGE IN CONTACT ANGLE. EXAGGERATED FOR CLARITY.

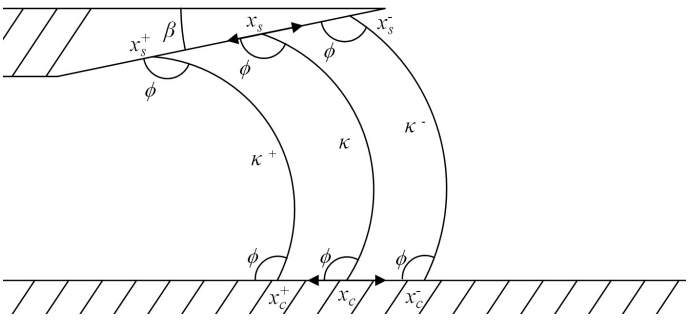

FIGURE 4. MENISCUS MOTION WHEN THE CONTACT ANGLE IS FIXED AND CURVATURE CHANGE IS ACCOMMODATED BY A CHANGE IN CONTACT LINE. EXAGGERATED FOR CLARITY.

Contact Angle

Contrary to popular belief, the contact angle is not fixed for a specific gas-liquid-solid interface, and is dependent on the molecular and dynamic conditions of the contact region. Tavana and Neumann [3] investigated the effect of molecular forces on the quasi-static meniscus. They found a variety of factors, including molecule shape and size which affected the contact an-

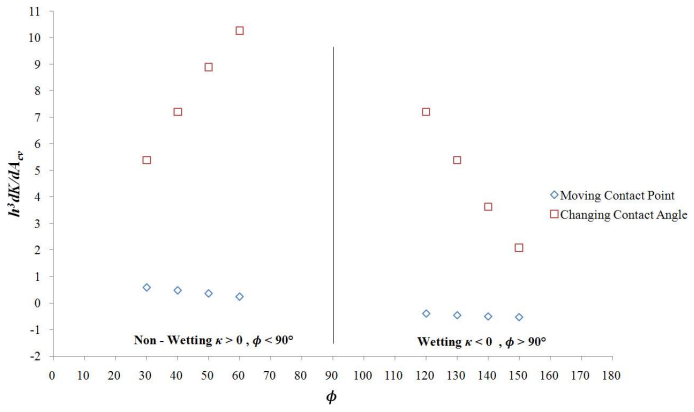

FIGURE 5. MENISCUS STIFFNESS, WHICH IS DETERMINED BY THE CONTACT ANGLE FOR THE RECESSED CASES. EXPERIMENTAL STIFFNESS VALUES SHOULD FALL BETWEEN THE TWO LIMITS.

gle. In addition, they found that the wetting time would change the interfacial properties of the contact region, changing the contact angle. The works of Erbil et al. [4], Hennig et al. [5] and Lam et al. [6] all show wetting time dependence on contact angle. In particular, Hennig et al. [5] found the contact angle for water in his experiments to vary up to 4^o due to wetting time effects. In addition, the prior authors [4–6] saw a significant difference in contact angle for the advancing and recessing meniscus. Hennig et al. [5], using water, reported a difference of 40^o between the advancing and retreating contact angle. They also show that when the contact angle is within the bounds of $\phi_a < \phi < \phi_r$, the contact line does not move.

Considering the meniscus behaviour just described, a stationary contact line model would apply where the substrate is stationary and the changes in curvature are small enough that the contact angle remains in the interval $\phi_a < \phi < \phi_r$. This would correspond to the present stationary substrate models under some circumstances. The case of constant contact angle would correspond to the case of the tangentially moving substrate, with $\phi = \phi_a$ or $\phi = \phi_r$. It would also apply to the stationary substrate case at large amplitudes of oscillation of curvature near the limits where $\phi > \phi_a$ or $\phi < \phi_r$. Such large amplitude oscillations would therefore have a intermittent stiffness.

In practice the substrate may also be moving in the normal direction to the substrate, due to background vibration, as in the work of Noblin et al. [7]. They investigated the contact motion of vibrated sessile drops and found the contact condition to be dependent on the local normal acceleration, a. They offer two thresholds for contact line motion, described in Eqn. 4 and Eqn. 5.

$$\frac{a}{g} > \frac{\lambda}{(1-\cos\phi_e)} \tag{4}$$

$$\frac{a}{g} > \frac{4\lambda}{\pi(1-\cos\phi_e)} \tag{5}$$

Where

$$\cos\phi_e = (\cos\phi_r + \cos\phi_a)/2$$

and

$$\lambda = 2(\cos\phi_e - \cos\phi_a) = 2(\cos\phi_r - \cos\phi_e)$$

Equations 4 and 5 compare the contact angle range with the acceleration of the surface. Equation 4 is the lower limit for contact line motion, bellow this only contact angle motion occurs. Once Eqn. 4 is exceeded, a portion of the oscillation period consists of contact line motion, during peak acceleration. Equation 5 is the theoretical limit for pure slip (contact line) motion. Pure slip is not possible for oscillating motion since the contact angle must change from advancing to receding at the apex, but for high accelerations the non-slip time is relatively short.

Based on the discussed contact region behaviour, we expect to see contact angle motion for small amplitude excitations used in natural frequency testing. Flow excited testing should exhibit both contact angle and contact line motion; the mixture being dependent on the flow rate, preferring contact angle motion for low flow and contact line motion for high flow experiments due to its large amplitude.

EXPERIMENTAL APPARATUS

The experimental apparatus for testing natural frequency is shown in Fig. 8 and consists of a removable scaled channel section, containing the meniscus, which is attached to a larger discharge tank with a free surface. The channel region is under partial vacuum with the free surface adjusted by adding or removing fluid to position the meniscus under the step, which is open to atmosphere on the obverse side. In testing, a syringe, connected to the discharge tank, is pulled to provide a change in fluid level which excites the meniscus. Natural frequency tests were performed with both water and mercury as the working fluid; a separate, identical apparatus being used for each fluid to prevent contamination.

Flow excited tests were also conducted for water. The water flow tests use the same apparatus as the natural frequency water tests, with the addition of a flow circuit and flow straightening section, as shown in Fig. 9.

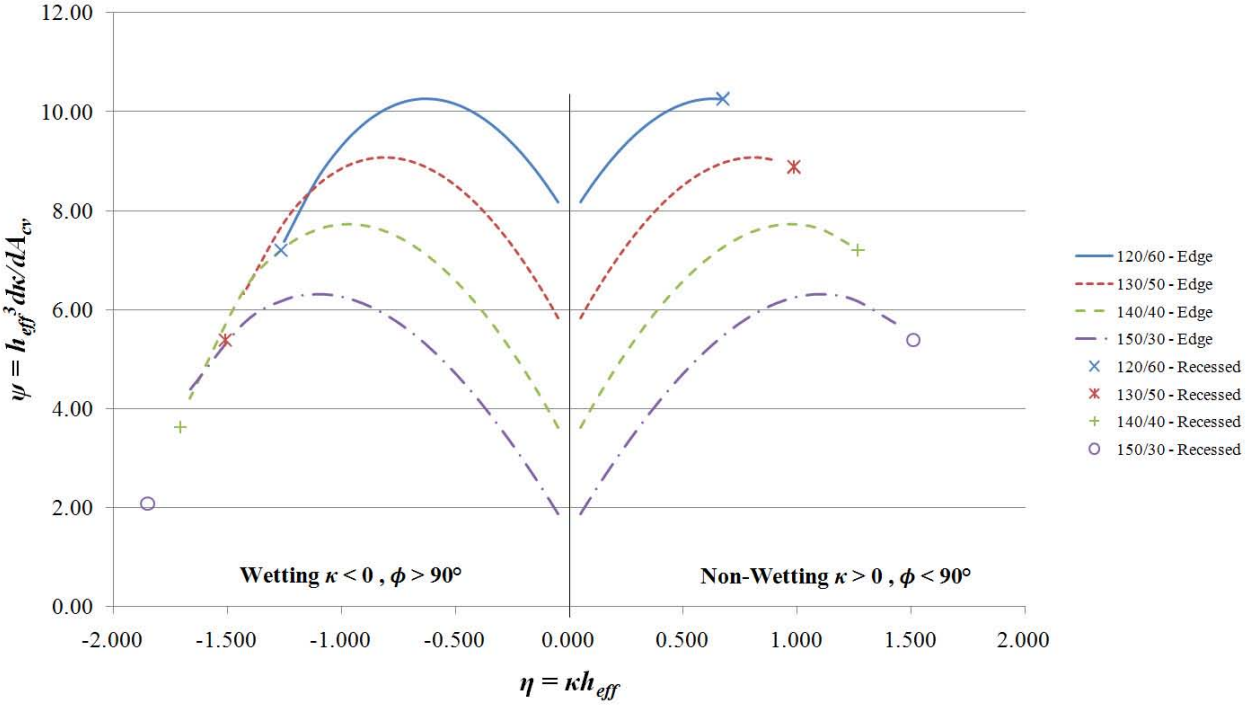

FIGURE 6. MENISCUS STIFFNESS AS A FUNCTION OF DIMENSIONLESS HEAD, η, AND CONTACT ANGLE, ϕ, FOR THE FIXED CONTACT LINE CASE. $\beta = 20^o$.

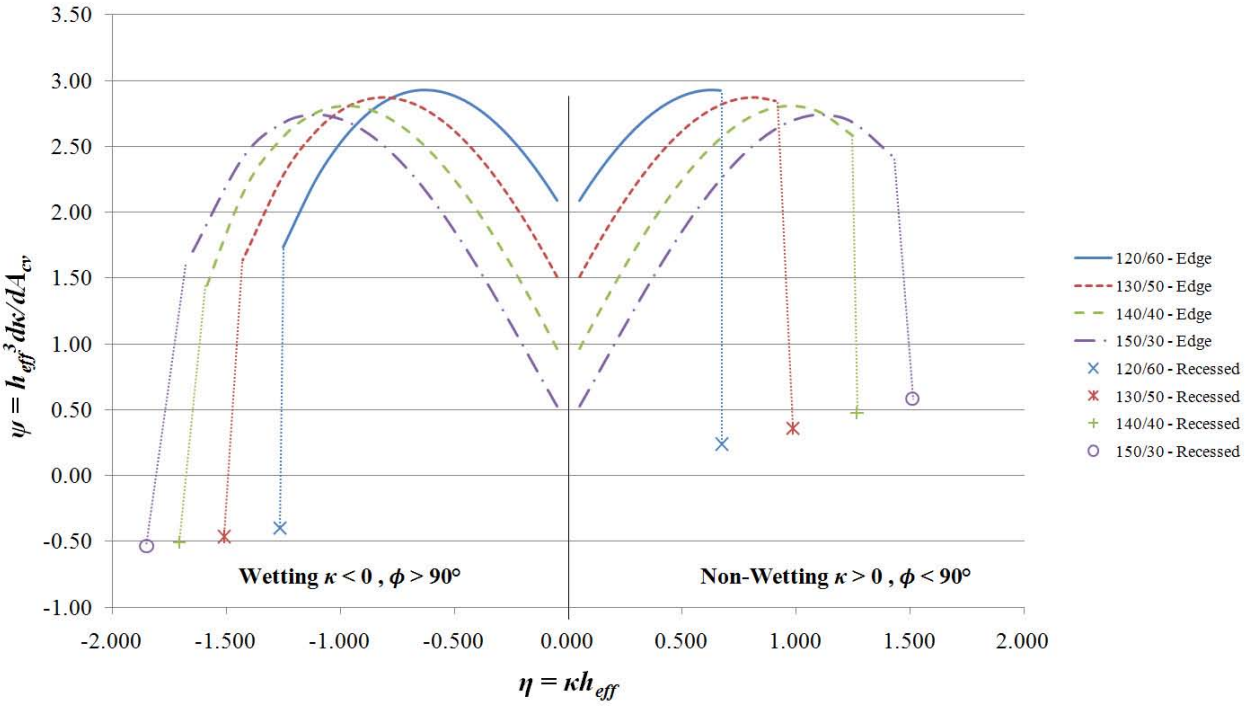

FIGURE 7. MENISCUS STIFFNESS AS A FUNCTION OF DIMENSIONLESS HEAD, η, AND CONTACT ANGLE, ϕ, FOR THE FIXED CONTACT ANGLE CASE. $\beta = 20^o$.

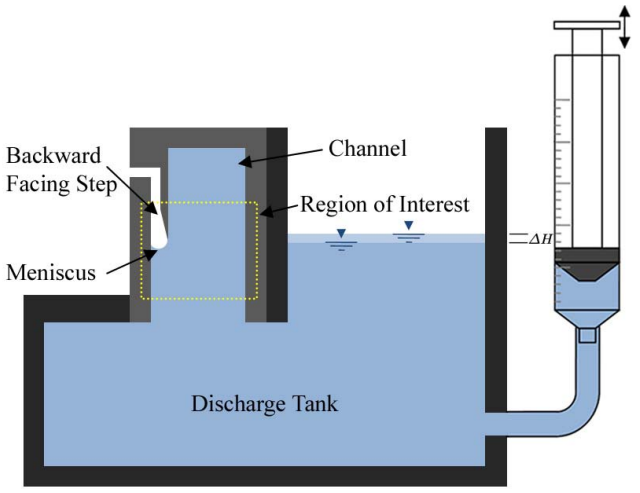

FIGURE 8. EXPERIMENTAL MODEL FOR NATURAL FREQUENCY TESTS. THE DASHED REGION INDICATES THE LOCATION OF THE BACKWARD FACING STEP AND MENISCUS.

Both Fig. 8 and Fig. 9 outline the region of interest, which contains the backward-facing step and meniscus and is depicted in Fig. 10. Table 1 describes the geometric dimensions of the model and Tab. 2 gives the fluid properties and flow ranges, where applicable, for water and mercury testing. Note that the channel slenderness, I, is calculated using the effective channel length, which is defined in Eqn. 6; the exit factor of 0.82 is for a flanged opening from Pierce [8] pp 345-349.

$$L_{eff} = L_{nom} + 0.82 D_{h_2} \tag{6}$$

where D_{h_2} is the hydraulic diameter of the post step region, defined as:

$$D_{h_2} = \frac{4h_2 d}{2(h_2 + d)}$$

EXPERIMENTAL METHOD

The meniscus response to natural frequency and flow excited testing is captured using high-speed videography of the meniscus region while being back lit, producing high contrast images like the one in Fig. 11. The step height in the image is 3.5 mm and the small size preserves the near circular shape of the meniscus assumed in the development of Eqn. 1.

Video frames were captured at 200 Hz in the natural frequency tests and at 24 Hz for flow excited testing. The low frame rate was used for the flow tests to extend the duration of the observation, which was necessary because of the random character of the meniscus motion. Each frame of a video compilation was processed using a MATLAB algorithm to calculate the location of the meniscus surface based on abrupt changes in contrast and user identified boundaries (the wall and step). The meniscus boundary is identified and a circular arc is fit to it. From this arc the curvature, contact points and contact angles are calculated, as is the area behind (above) the meniscus. In the case of the natural frequency testing, this gives us time-resolved values for the meniscus parameters. Time resolution is not required for the flow excited testing as we are only concerned with a statistical

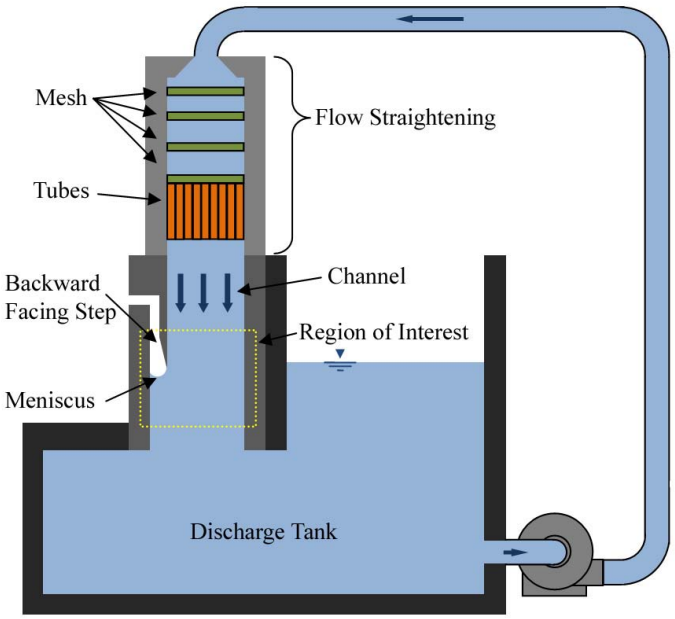

FIGURE 9. EXPERIMENTAL MODEL FOR FLOW EXCITED TESTING. THE MODEL IS THE SAME AS THAT FOR THE NATURAL FREQUENCY TESTS WITH THE ADDITION OF THE FLOW CIRCUIT.

TABLE 1. GEOMETRIC VARIABLES FOR THE WATER AND MERCURY MODEL.

Geometric Variables			Water (Wetting)	Mercury (Non-wetting)
h	Step Height	$[mm]$	3.5	
h_1	Pre-Step Height	$[mm]$	$4.4, 10.3, 16.7, 22.6$	
h_2	Post-Step Height	$[mm]$	$7.9, 13.8, 20.2, 26.1$	
L	Channel Length	$[mm]$	90	60
d	Channel Width	$[mm]$	50	
ϕ	Contact Angle	$[deg]$	$130-150$	$30-50$

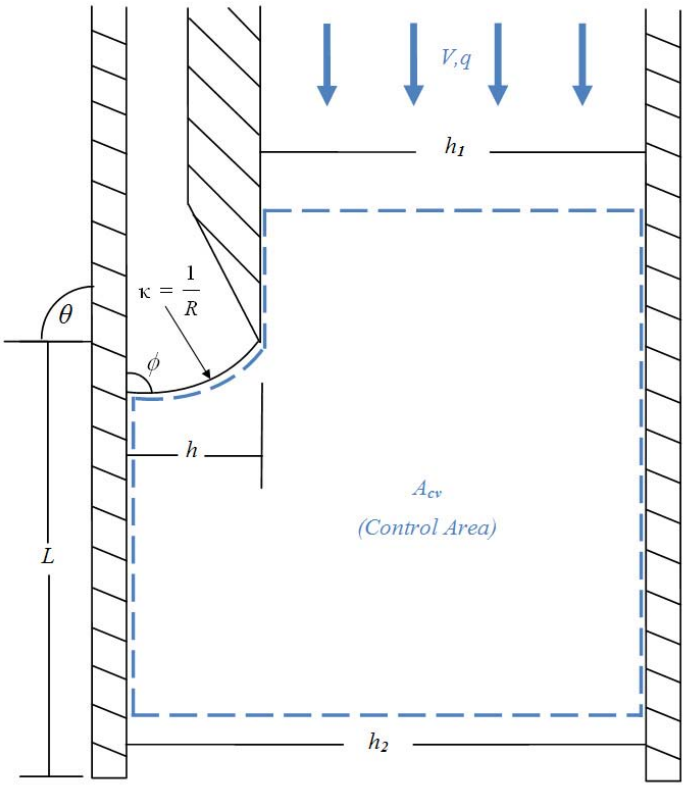

FIGURE 10. REGION OF INTEREST IN THE EXPERIMENTAL MODEL. THE DASHED REGION SPECIFIES THE CONTROL AREA IN THE ANALYSIS OF GERBER ET AL. [2] WHERE MOVEMENT OF THE MENISCUS UNDER THE STEP CAUSES A CHANGE IN THE CONTROL AREA SIZE WITH A CHANGE OF MENISCUS RADIUS.

TABLE 2. PROCESS VARIABLES FOR THE WATER AND MERCURY MODEL.

Process Variables			Water	Mercury
			(Wetting)	(Non-wetting)
ρ	Density	$[kg/m^3]$	1000	13579
ν	Viscosity	$[m^2/s]$	$1.0\text{x}10^{-6}$	$0.114\text{x}10^{-6}$
σ	Surface Tension	$[N/m]$	0.073	0.487
q	Flow Rate (per unit depth)	$[m^2/s]$	$0.002-0.01$	–
U	Channel Velocity	$[m/s]$	$0.04-0.20$	–

description although the Nyquist criterion was observed in this case. The specific camera settings used for testing are given in Tab. 3.

FIGURE 11. WATER-AIR MENISCUS UNDERNEATH THE STEP DURING A NATURAL FREQUENCY TEST. THE STEP HEIGHT IS 3.5 mm FOR COMPARISON.

EXPERIMENTAL RESULTS

Natural Frequency

A typical natural frequency response for a water test is shown in Fig. 12 where the area behind the meniscus, A_{cv}, is plotted versus time. A clear dominant frequency and exponential decay can be seen. The area determined from the arc fitted to the meniscus is compared to a direct numerical integration of the area from the video frame. The area calculated directly from the video frame is considered to be the most accurate indicator of meniscus motion and is used to calculate the natural frequency. From the fitted arc the contact lines and angles are calculated, as is the effective step height. The excellent agreement between the area calculated by the two methods confers confidence in the contact line, angle and effective step height values.

Natural frequency experiments for water were conducted using four different slenderness ratios based on the channel length and post-step widths given in Tab. 1. For each geometry, the natural frequency of the recessed meniscus was determined from

TABLE 3. VIDEO SETTINGS FOR THE NATURAL FREQUENCY AND FLOW EXCITED TESTING.

Camera Setting		Water		Mercury
		(Flow)	(Natural Frequency)	
Frames per second	$[-]$	24	200	200
Frame size	$[pixel]$	356x456	356x456	356x456
Duration	$[s]$	80	8	5
Number of frames	$[-]$	1920	1600	1000
Exposure Time	$[ms]$	4.0	4.0	4.0
Aperture	$[1/f]$	8	8	8

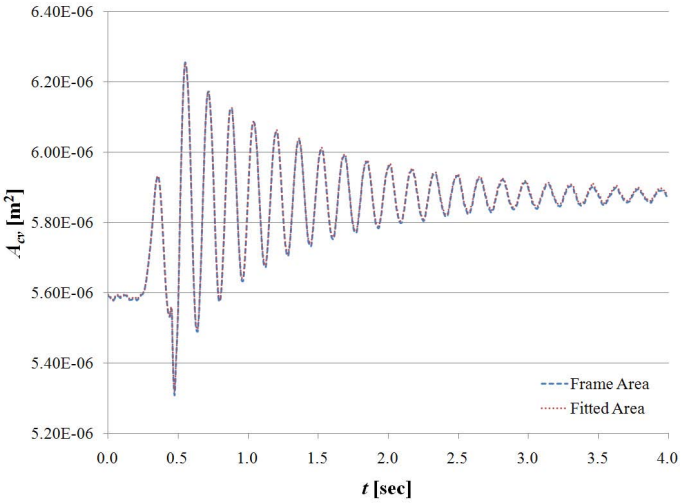

FIGURE 12. RESPONSE FROM A TYPICAL NATURAL FREQUENCY TEST USING WATER, PLOTTING THE AREA BEHIND THE MENISCUS, A_{cv}.

tests conducted at various effective step heights which were not known *a priori* but were calculated from the fitted meniscus arc. The results for natural frequency testing with water are shown in Fig. 13.

A curve is fitted to the data for each test geometry shown in Fig. 13 based on Eqn. 7 with the stiffness, ψ, fitted using a least-squares method. Considering the good agreement obtained, one would conclude that the form of Eqn. 7 is correct for predicting the meniscus natural frequency. The range of stiffness that suits this purpose is 2.72 to 4.91. If we compare these stiffness values to the changing contact angle points for the wetting case of Fig. 5, they correspond to contact angles of $149^o > \phi > 135^o$ with a mean of 141.25^o and total range of 14^o. The sensitivity of stiffness to contact angle is high; however, the contact angle range is within the expected values and consistent with the work of Tavana and Neumann [3], who state that contact regions involving water are particularly susceptible to molecular effects. A specific

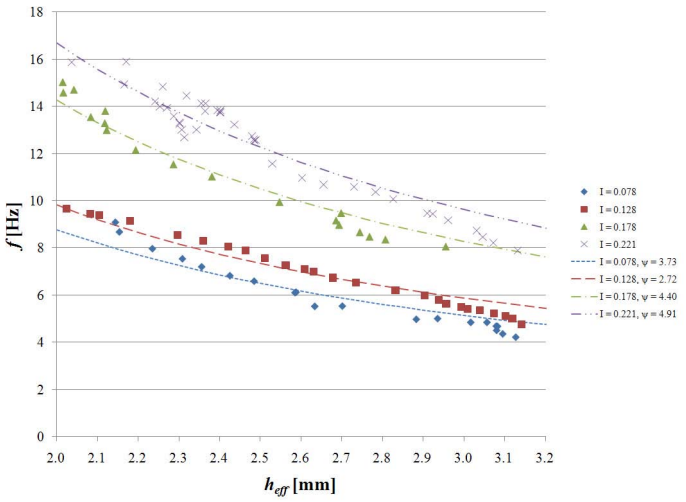

FIGURE 13. RESULTS OF THE NATURAL FREQUENCY TESTS FOR WATER WITH FOUR DIFFERENT SLENDERNESS VALUES. CURVE FITS ARE FOR A CONSTANT STIFFNESS, ψ.

example is given in the work of Hennig et al. [5] where the contact angle of water on a polyimide surface was found to change by 4^o due to wetting time during testing under very controlled conditions. Experimental confirmation of the fitted stiffnesses could involve observed meniscus behaviour from the video data and this will be pursued in the future.

$$f_n = \frac{1}{2\pi}\sqrt{I\left(\frac{\sigma}{\rho h_{eff}^3}\psi + \frac{g}{h_{eff}}\right)} \tag{7}$$

Figure 14 shows the natural frequency results for testing with mercury for three different slenderness values. Similar to Fig. 13, the stiffness values are fitted to the experimental data and fall within the expected range in Fig. 5 for non-wetting conditions. This verifies that Eqn. 7 is valid for both the wetting and non-wetting cases and could apply to meniscus oscillations in aluminium casing.

Flow Excitation

Flow excitation tests were conducted with water for the velocity range given in Tab. 2. The geometry used had $I = 0.128$ where $h_2 = 13.8mm$ and $L = 90mm$ ($L_{eff} = 107.7mm$), and an effective step height of approximately 3.1mm. The spectra of the flow data are shown in Fig. 15

From Fig. 15 we see that the frequency peaks for the flow tests are all around 5 Hz, which agrees with the natural frequency results for this geometry, shown in Fig. 13.

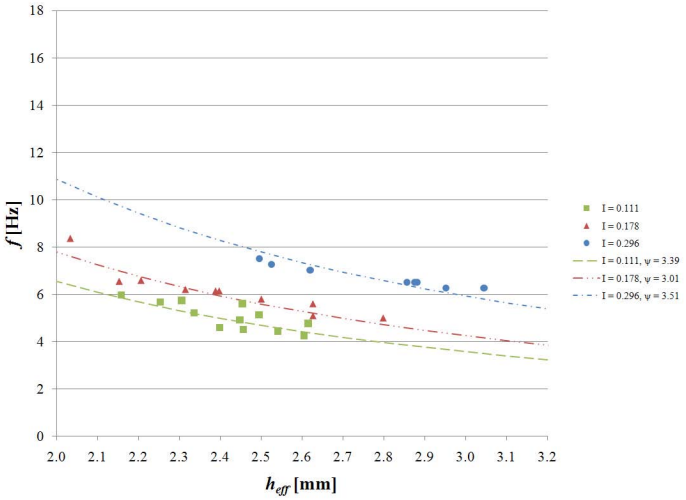

FIGURE 14. RESULTS OF THE NATURAL FREQUENCY TESTS FOR MERCURY WITH THREE DIFFERENT SLENDERNESS VALUES. CURVE FITS ARE FOR A CONSTANT STIFFNESS, ψ.

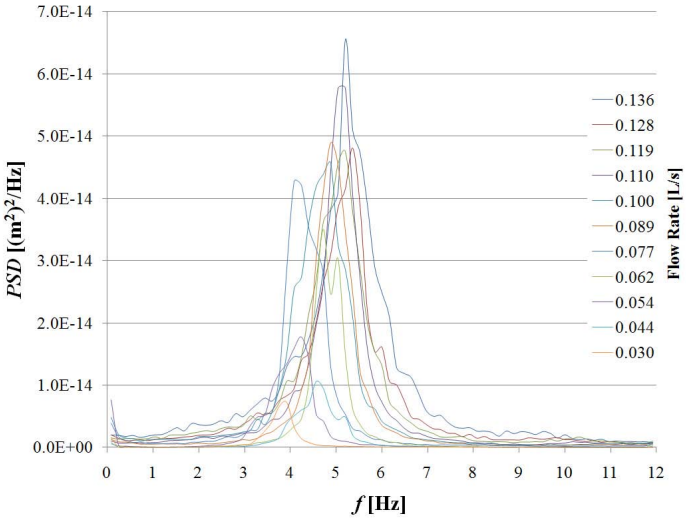

FIGURE 15. POWER SPECTRAL DENSITY (PSD) OF THE CALCULATED MENISCUS AREA, A_{cv} FOR ALL FLOW TESTS.

Figure 16 plots the energy of the meniscus oscillations, based on the fluctuating component of the flow velocity, which is calculated from the area behind the meniscus, A_{cv}, as described in Eqn. 8

$$u = -\frac{1}{h_2}\frac{dA_{cv}}{dt} \tag{8}$$

Figure 16 shows a linear dependence of meniscus energy on

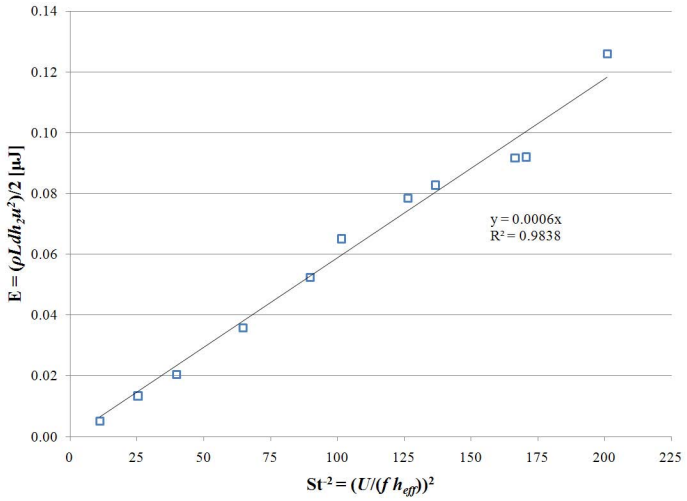

FIGURE 16. ENERGY CONTAINED WITHIN THE MENISCUS OSCILLATIONS AS A FUNCTION OF SQUARED INVERSE STROUHAL NUMBER.

the inverse squared Strouhal number. This is typical flow induced excitation being proportional to the velocity squared.

Figure 17 shows the probability density function of the fluctuating component of channel velocity (derived from A_{cv}), normalized by its standard deviation, σ_u. As the figure indicates, the profiles collapse for all of the mean flow rates investigated. Statistical similarity of the fluctuating component of the flow, and hence the meniscus motion, is interesting as it allows the statistical prediction of extreme meniscus positions, which may lead to meniscus collapse.

CONCLUSION

An isothermal model of the aluminium continuous strip casting process was used to observe the motion of an air-liquid meniscus, representing an air-aluminium meniscus in the casting process, and calculate its natural frequency of oscillation. Natural frequency tests were conducted using both water and mercury as the working fluids, water having a wetting contact angle with the substrate, whereas mercury was non-wetting, similar to the casting case with aluminium. In both cases, the experimental results coincided with the expectations of theory [1, 2] (Eqn. 7), which is repeated here:

$$f_n = \frac{1}{2\pi}\sqrt{I\left(\frac{\sigma}{\rho h_{eff}^3}\psi + \frac{g}{h_{eff}}\right)} \tag{9}$$

Flow excited tests were performed for water where the meniscus frequency was found to be independent of flow rate and

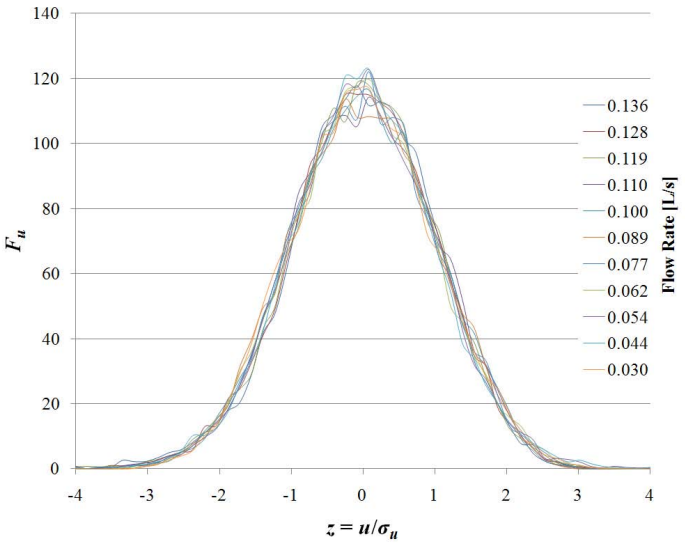

FIGURE 17. PDF OF THE VELOCITY FLUCTUATIONS IN THE FLOW, DERIVED FROM THE CALCULATED MENISCUS AREA, A_{cv}. THE PROFILE IS THE SAME FOR ALL FLOW RATES WHEN NORMALIZED BY THE STANDARD DEVIATION.

equal to the natural frequency. In addition, the energy of meniscus excitation was found to increase linearly with the inverse squared Strouhal number, indicating that excitation was broadband in nature. Furthermore, the probability density profile of the fluctuating component of flow velocity, which is directly related to meniscus amplitude, was shown to collapse to one profile when normalized by the standard deviation. This allows the probability of extreme meniscus positions, which may result in casting failure, to be calculated based on nominal casting rate and geometry.

References

[1] McLeod, I. M., 2006. "An isothermal water model of continuous aluminium sheet casting". Msce thesis, University of New Brunswick, Fredericton, NB, June.

[2] Gerber, A. G., Holloway, A. G. L., and Ng, C., 2007. "A model of unsteady response of a backward-facing compliant step". *International Journal for Numerical Methods in Fluids,* ***55***(1), September, pp. 57–80.

[3] Tavana, H., and Neumann, A. W., 2007. "Recent progress in the determination of solid surface tensions from contact angles". *Advances in Colloid and Interface Science,* ***132***, pp. 1–32.

[4] Erbil, H. Y., McHale, G., Rowan, S. M., and Newton, M. I., 1999. "Determination of the receding contact angle of sessile drops on polymer surfaces by evaporation". *Langmuir,* ***15***, pp. 7378–7385.

[5] Hennig, A., Eichhorn, K. J., Staudinger, U., Sahre, K., Rogalli, M., Stamm, M., Neumann, A. W., and Grundke, K., 2004. "Contact angle hysteresis: Study by dynamic cycling contact angle measurements and variable angle spectroscopic ellipsometry on polyimide". *Langmuir,* ***20***, pp. 6685–6691.

[6] Lam, C. N. C., Ko, R. H. Y., Yu, L. M. Y., Ng, A., Li, D., Hair, M. L., and Neumann, A. W., 2001. "Dynamic cycling contact angle measurements: Study of advancing and receding contact angles". *Journal of Colloid and Interface Science,* ***243***, pp. 208–218.

[7] Noblin, X., Buguin, A., and Brochard-Wyart, F., 2004. "Vibrated sessile drops: Transition between pinned and mobile contact line oscillations". *The European Physical Journal E,* ***14***, pp. 395–404.

[8] Pierce, A. D., 1991. *Acoustics, An Introduction to Its Physical Principles and Applications*. Acoustical Society of America.